Thermal properties, crystal structures, and photoreactivity of Ru-containing ionic liquids with sulfur-containing substituents

Sumitani, Ryo

Mochida, Tomoyuki

(Citation)
Journal of Molecular Liquids,344:117784

(Issue Date)
2021-12-15

(Resource Type)
journal article

(Version)
Accepted Manuscript

(URL)
https://hdl.handle.net/20.500.14094/90008783

Thermal Properties, Crystal Structures, and Photoreactivity of Ru-Containing Ionic Liquids with Sulfur-Containing Substituents

Ryo Sumitani[a] and Tomoyuki Mochida[a,b]*

[a]*Department of Chemistry, Graduate School of Science, Kobe University, 1-1 Rokkodai, Nada, Kobe, Hyogo 657-8501, Japan*

[b]*Research Center for Membrane and Film Technology, Kobe University, 1-1 Rokkodai, Nada, Kobe, Hyogo 657-8501, Japan*

*Corresponding author.

E-mail address: tmochida@platinum.kobe-u.ac.jp (T. Mochida)

Graphical abstract

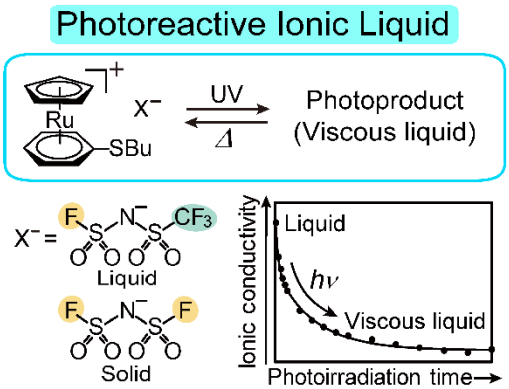

Ruthenium-containing organometallic ionic liquids with sulfur-containing substituents were developed, and the correlation between the structure and melting point was investigated. The liquid salt exhibited reversible structural transformation upon the application of light and heat, accompanied by a change in the ionic conductivity.

Highlights

- Ru-containing organometallic ionic liquids with butylthio substituents were synthesized.
- The effects of different anions on the melting point and crystal structure were investigated.
- The FSA salt exhibited a relatively high melting point owing to its dense crystal packing.
- The FTA salt underwent a photochemical reaction accompanied by conductivity changes.

ABSTRACT

Ionic liquids containing cationic Ru sandwich complexes exhibit diverse photochemical reactions. To investigate the effect of sulfur-containing substituents and anions on the physical properties and chemical reactivity of ionic liquids, we synthesized ionic liquids $[Ru(C_5H_5)(C_6H_5SBu)]X$ (X = anion) containing *n*-butylthio substituents. The salts with PF_6 and $(SO_2F)_2N^-$ (FSA) anions were solids with melting points of 74 and 64 °C, respectively. X-ray crystallography of the FSA salt indicated that its relatively high melting point was because of its dense crystal packing. The FSA salt exhibited an order–disorder phase transition at −97 °C. The salt with the unsymmetrical $(SO_2F)(SO_2CF_3)N^-$ (FTA) anion was a liquid and exhibited a glass transition at −79 °C. Upon UV photoirradiation, the liquid underwent the structural transformation of the cation with low conversion and transformed to a more viscous liquid with lower ionic conductivity. The reaction was reversed upon heating via an intermediate state.

Keywords Ionic liquid; Crystal structure; Ruthenium complex; Phase transition; Photochemical reaction; Ionic conductivity

1. Introduction

Ionic liquids (ILs) have gained significant attention because of their properties such as negligible vapor pressure, flame retardancy, and high ionic conductivity [1]. In recent years, extensive studies have been conducted on ILs for their application as electrolytes and solvents. Furthermore, several task-specific ILs exhibiting unique properties have been synthesized [1]. Metal-containing cations and anions are effective in incorporating the properties of the metal complexes into their ILs [2]. We have previously synthesized ILs containing cationic organometallic [3] and chelate complexes [4], which exhibited various properties such as magnetism and chemical reactivity.

In recent years, modification of the physical properties of ILs by external stimuli has gained attention because this strategy expands their scope of electronic applications [5]. We have previously developed photoreactive Ru-containing ILs that exhibit reversible changes in ionic conductivity and mechanical properties in response to the application of light and heat. Fig. 1 [6a] shows a schematic of the photochemical and thermal reactions for an IL containing three cyanoalkyl substituents and a $(SO_2F)_2N^-$ (FSA) anion. Upon UV photoirradiation, dissociation of the arene ligand occurs, followed by the coordination of the three cyano groups to the metal ion to form a coordination polymer (Fig. 1). The reverse reaction occurs upon heating. The mechanism for the photochemical reaction is based on the reactivity of the cationic Ru sandwich complexes [7], and coordinating substituents are required for such reactions to occur. For example, **2-FSA** (Fig. 2a, middle; X = FSA) transforms to a viscous liquid upon UV irradiation, which predominantly consists of a trinuclear complex bridged via -CN–Ru bonds [6b]. However, **3-FSA** with no coordinating substituent (Fig. 2a, right; X = FSA) is photochemically inert [3b]. Although cyano substituents are effective for these reactions [8], the investigation of other substituents is significant.

In this study, we investigated the effect of a sulfur-containing substituent in the cation on

the photochemical reaction of ILs. We synthesized ionic liquids [CpRu(C_6H_5SBu)]X (Cp = C_5H_5, X = anion), where the anions were PF_6, FSA, and FTA ($(SO_2F)(SO_2CF_3)N^-$), and their respective salts are abbreviated as **1-PF$_6$**, **1-FSA**, and **1-FTA**. We used the unsymmetric FTA anion [9] because **1-FSA** exhibited a relatively high melting point. The effects of the anions on the melting point and crystal structure were discussed. Furthermore, we investigated the photochemical reaction of liquid **1-FTA**, which is accompanied by a change in ionic conductivity.

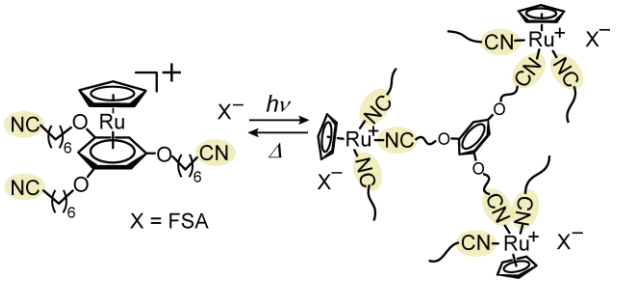

Fig. 1. Reversible structural transformation of a Ru sandwich complex upon the application of light and heat [6a].

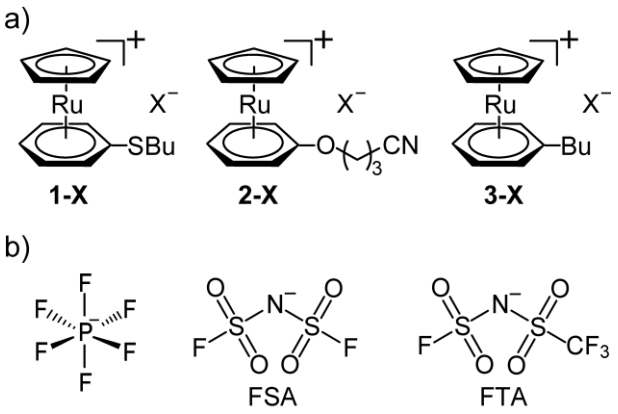

Fig. 2. Structural formulae of (a) **1-X**, **2-X**, and **3-X** (X = anion) and (b) the anions used in this study. **2-X** and **3-X** (X = PF_6, FSA) were used in previous studies [3b, 11].

2. Results and Discussion

2.1. Synthesis and Thermal properties

1-PF$_6$ was synthesized by the reaction of [CpRu(CH_3CN)$_3$]PF_6 with butylthiobenzene,

whereas **1-FSA** and **1-FTA** were obtained by anion exchange from the PF_6 salt. The results of the differential scanning calorimetry (DSC) of the salts are summarized in Table 1. **1-PF$_6$** and **1-FSA** were colorless crystals, whereas **1-FTA** was a pale orange liquid; all these salts were regarded as ILs with melting points below 100 °C.

1-PF$_6$ melted at 74.0 °C, and no crystallization occurred upon cooling from the melt, exhibiting a glass transition at −45 °C. Upon heating from the glassy state, it changed to a liquid, and then cold crystallization occurred over a temperature range of −10–35 °C. The ratio of glass transition temperature (T_g) to melting point (T_m) was 0.66, which was in agreement with the empirical relationship ($T_g/T_m = 2/3$) for molecular liquids including ILs [10]. The DSC curve of the salt is shown in Fig. S1 (ESI).

1-FSA melted at 64.4 °C. Unlike **1-PF$_6$**, this salt crystallized at approximately −20 °C upon cooling from the melt. This behavior was in contrast with that of **2-FSA** and **3-FSA**, which exhibit only glass transition (at −60 and −82 °C, respectively) [3b,11]. In addition, **1-FSA** exhibited a phase transition at −96.7 °C (ΔS = 2.9 J K^{-1} mol^{-1}, Fig. 3), which was analyzed by X-ray crystallography to be an order–disorder phase transition (see below).

1-FTA was a liquid at ambient temperature, and no crystallization occurred upon cooling. The liquid exhibited glass transition at −79 °C. This indicates that the FTA anion is effective in producing a Ru-containing organometallic IL with a low melting point.

To investigate the thermal stability of the cation, thermogravimetry-differential thermal analysis (TG-DTA) measurement of **1-FSA** was performed (Fig. S2, ESI). The decomposition temperature of this salt was 234 °C (at 3% weight loss, 10 K min^{-1}), which was 20–30 K lower than those of **2-FSA** (253 °C [3b]) and **3-FSA** (265 °C [11]). **1-FSA** exhibited a weight loss of ~30 wt% at 210–280 °C, which corresponds to the loss of the arene ligand (calculated value: 32 wt%). Therefore, the introduction of the butylthio substituent decreased the thermal stability of the cation.

Table 1. Glass transition temperatures (T_g), melting points (T_m), melting enthalpies (ΔH_m), and melting entropies (ΔS_m) of the synthesized ILs.

	T_g (°C)	T_m (°C)	ΔH_m (kJ mol^{-1})	ΔS_m (J K^{-1} mol^{-1})
1-PF$_6$	–45	74.0	32.1	92.4
1-FSA		64.4	11.7	34.6
1-FTA	–79			

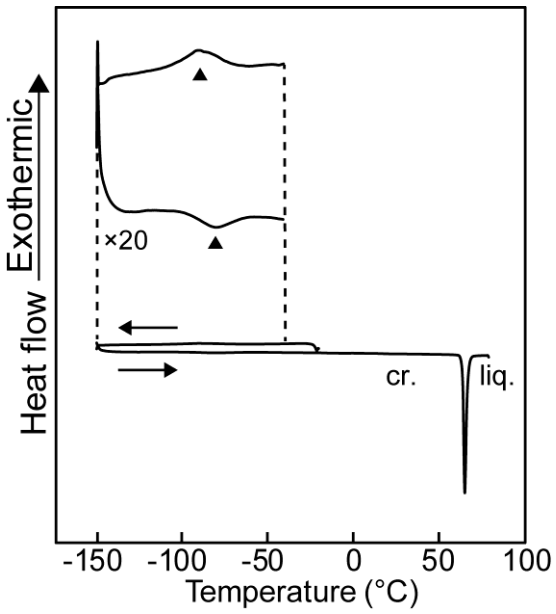

Fig. 3. DSC curve of **1-FSA**, where liq. and cr. are the liquid and crystal phases, respectively. A magnified view of the curve around the low-temperature phase transition (T_c) is also shown.

2.2. Melting points vs. packing efficiency

FSA salts typically exhibit significantly lower melting points than the corresponding PF_6 salts. However, the melting point of **1-FSA** (T_m = 64.4 °C) was closer to that of **1-PF$_6$** (T_m = 74.0 °C) than expected. To investigate the reason, we examined the packing efficiency of the salts in the solid state.

The crystal structures of **1-PF$_6$** and **1-FSA** were determined at −183 °C through X-ray crystallography (see below), and their packing indices were calculated using the Platon software

(Table 2). The packing indices of other Ru-containing complexes calculated from their structural data are summarized in Table 2. The FSA salts exhibited lower packing indices than the PF_6 salts owing to the asymmetry of the PF_6 anion, which was consistent with their low melting points. However, the comparison is vague as only a few PF_6 and FSA salts have been structurally characterized. The packing index of **1-FSA** (73.6%) was significantly higher than those of the other FSA salts (69%–71%), which could be accountable for its relatively high melting point (compared to [CpRu(PhR)]FSA: T_m = 33.5 °C (R = OCH_2OMe [3b]), T_m = 16.9 °C (R = Et [11]), and the salts listed in Table 2) and tendency to readily crystallize when cooled from the melt. In addition, the lower packing index of **1-PF$_6$** (71.3%) than that of structurally similar PF_6 salts (Table 2) could be accountable for its lower melting point.

Table 2. Packing indices and melting points (T_m) of **1-PF$_6$**, **1-FSA**, and related salts

Salts		Packing index (%)[a]	T_m (°C)	Reference
PF_6 salts	**1-PF$_6$**	71.3	74.0	this study
	3-PF$_6$	74.8	87.0	[3b]
	[CpRu($PhOCH_2OMe$)]PF_6	74.1	109.1	[3b]
FSA salts	**1-FSA**	73.6	64.4	this study
	[CpRu($PhOC_9H_{19}$)]FSA	69.5	57.9	[12a]
	[CpRu{1,2,3-$C_6H_3(OEt)_3$}]FSA	68.6	59.8	[12b]
	[CpRu{1,3,5-$C_6H_3(C_3H_6CN)_3$}]FSA	71.4	86.9	[6c]

a) Calculated for the structures at −183 °C (**1-PF$_6$** and **1-FSA**) and at −173 °C (other salts).

2.3. Crystal structures

X-ray crystallography of **1-PF$_6$** and **1-FSA** indicated significantly similar packing to each other. The low-temperature phase transition of **1-FSA** was an order–disorder phase transition of the cations and anions.

X-ray crystallography of **1-PF$_6$** was performed at −183 °C; the packing diagram is shown in Fig. 4a. The compound crystallized in the space group $P\bar{1}$ (Z = 2), and the asymmetric unit contained a pair of cation and anion. The cations and anions were arranged alternately, and

every cation was surrounded by six anions. The PhSBu moieties were adjacent to each other between the cations although no π–π interactions were discerned.

X-ray crystallography of **1-FSA** was performed at −183 °C and 0 °C to investigate the nature of the phase transition at −97 °C. The packing diagrams at both temperatures are shown in Fig. 4b, which closely resembled that of **1-PF$_6$**. The space group was the same in both phases ($P\bar{1}$, Z = 2), and the asymmetric unit contained a pair of cation and anion. The molecular arrangements were almost identical at both temperatures, with larger thermal ellipsoids at 0 °C than at −183 °C. No disorder was discerned at −183 °C, whereas the cations and anions exhibited disorder at 0 °C. The Cp ring of the cation exhibited a two-fold rotational disorder at 0 °C with an occupancy ratio of 0.38:0.62. The anion adopted an ordered *transoid* structure at −183 °C, and the environments around the two SO_2F groups were different; there were short O···HC contacts between one of the SO_2F groups and the arene moieties of the neighboring cations, which were 0.2–0.4 Å shorter than the van der Waals distance. At 0 °C, the N atom and SO_2F moieties of the anion exhibited an extensive three-fold rotational disorder with an occupancy ratio of 0.53:0.27:0.20 (Fig. S3, ESI). FSA anions typically exhibit an order–disorder phase transition in the crystal [6c,13] although the disorder is generally two-fold; hence, the observed three-fold disorder was distinctive.

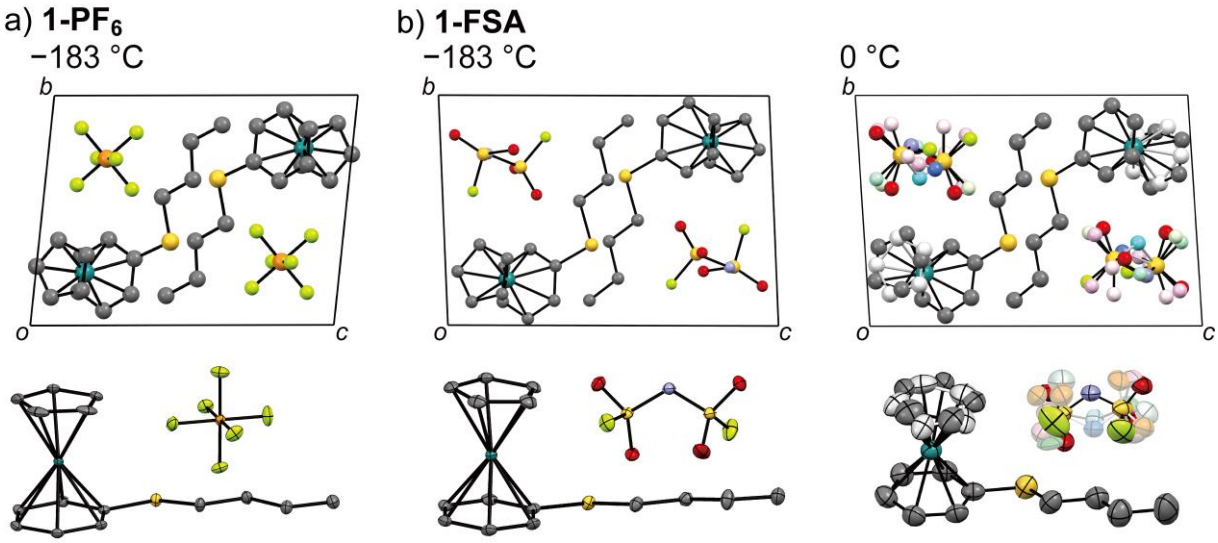

Fig. 4. Packing diagrams of (a) **1-PF$_6$** (−183 °C) and (b) **1-FSA** (−183 and 0 °C). The ORTEP diagrams of the molecular structures are shown below each figure. The disordered moieties are displayed in gray.

*2.4. Photoreactivity of **1-FTA***

The UV photoirradiation (365 nm, LED) of **1-FTA** for 30 min resulted in a mixture of photoproducts and unreacted species, and the pale orange liquid transformed to a yellow and more viscous liquid. The change in the UV-vis spectra due to photoirradiation can be observed in Fig. 5a, which shows a new absorption peak at approximately 410 nm. This observation, along with the changes in the ^{1}H NMR and IR spectra (Figs. S4 and S5, ESI), indicated that the sandwich structure transformed to a half-sandwich structure [6a]. A plausible structure of the dominant photoproduct, which is a dinuclear complex, is shown in Fig. 7 (product A). After photodissociation, the Ru ion accepts three donor atoms, namely, the dissociated ligand (PhSBu) and the undissociated cation and anion. Density functional theory (DFT) calculations indicated that the suggested structure was the most stable among plausible structures (Fig. S6, ESI). However, the structure could not be confirmed through ^{1}H NMR spectroscopy because of dissociation.

The amount (%) of photodissociated cations as a function of photoirradiation time was determined from the ^{1}H NMR spectra; the plot is shown in Fig. 6a. The amount was 22% in 45 min, which corresponded to a 43% yield of product A. This result indicates that the reaction is considerably less efficient than that of **2-FSA** (93% in 15 min [6b]). The low efficiency could be attributed to the UV-vis absorption of the photoproduct, which made the photoirradiation at 365 nm less effective, and a likely thermal reverse reaction during photoirradiation.

As the coordination ability of the sandwich complex ligand in product A is weak owing to its cationic nature, it could dissociate to produce product B, as shown in Fig. 7. The dissolution

of the yellow photoproduct in dichloromethane produced a yellow–green solution, which exhibited a UV-vis absorption peak at approximately 427 nm (Fig. S7, ESI). Furthermore, after removal of free ligands from product A through gel permeation chromatography (GPC), a peak was observed in the ESI-MS spectrum at m/z = 585.2495 (Na^+ adduct) that corresponded to product B. DFT calculations predicted that the structure of product B (Fig. S6, ESI) is similar to those of other Ru complexes with the *N*,*O*-chelate coordination of FSA [14]. However, we were unable to isolate the compound; thus, the peaks of the ^1H NMR and ESI-MS spectra could not be completely assigned.

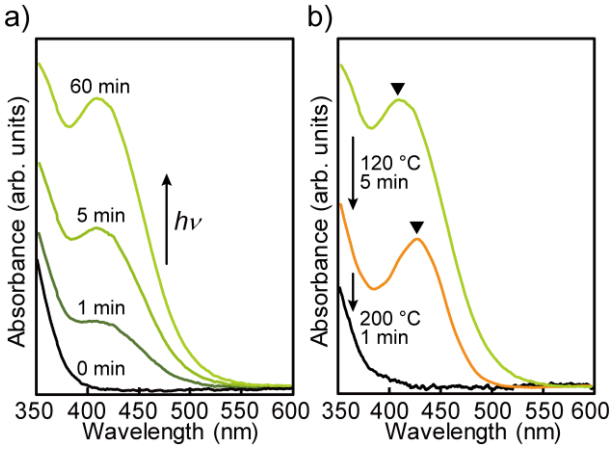

Fig. 5. UV-vis spectral changes upon (a) photoirradiation of **1-FTA** and (b) heating the photoproduct of **1-FTA**. The sample was sandwiched between two quartz plates to perform the measurements.

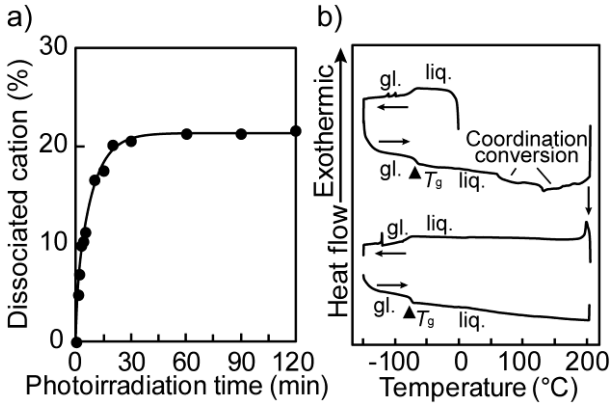

Fig. 6. (a) Amount (%) of the photodissociated cations observed for the photoreaction of **1-FTA** plotted as a function of photoirradiation time. (b) DSC curves (first and second cycles) of

the photoproduct of **1-FTA**.

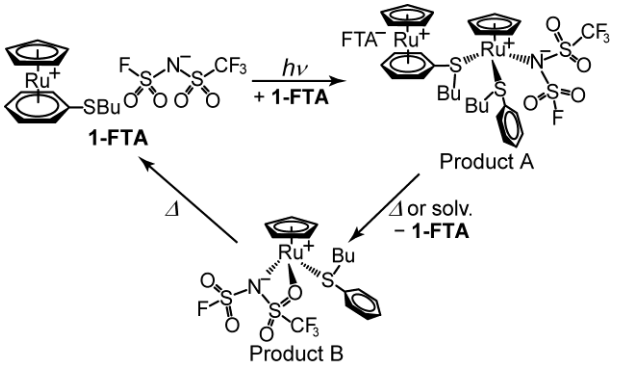

Fig. 7. Putative photochemical and thermal reactions of **1-FTA**.

*2.5. Thermal reaction of the photoproduct of **1-FTA***

The photoproduct of **1-FTA** transformed back to **1-FTA** via an intermediate state upon heating. After heating the photoproduct (λ_{max} = 410 nm) at 120 °C for 5 min, the UV–vis absorption peak shifted to 427 nm (Fig. 6b). Based on the results discussed in the previous section, we deduced that the intermediate contained cation-dissociated product B. After further heating at 200 °C for 1 min (or 120 °C for 1 h), **1-FTA** was completely recovered, and no UV-vis absorption peak was observed in the visible region. The recovery was further confirmed by the changes in the ^{1}H NMR spectrum (Fig. S4, ESI).

The thermal reaction of the photoproduct was analyzed by DSC (scan rate: 10 °C min^{-1}, Fig. 5b). During the first heating cycle, the photoproduct exhibited a glass transition at −72 °C and significantly broad endothermic peaks from 60–180 °C, which were attributed to the coordination transformation of the cation [6a]. The results were similar at a scan rate of 5 °C min^{-1}. Considering the reactivity of the photoproduct, we speculated that the broad peaks at approximately 80 and 140 °C corresponded to the transformation of product A to B and then to the original IL. The onset of decomposition at >180 °C was indicated by the occurrence of an exotherm. In the second cycle, a glass transition was observed at −77 °C, and the broad endothermic peaks at high temperatures were absent, which is consistent with the recovery of

1-FTA. The thermal reverse reaction occurred at a higher temperature range than that for the photoproduct shown in Fig. 1 (50–120 °C [6a]), which is attributed to the stronger S–Ru bond than the CN–Ru bond.

These results indicated that the photoreaction of the sulfur-containing IL was significantly different from those of the ILs containing cyano substituents. The photoreactivity and conversion of the sulfur-containing IL were low, and the photoproducts were likely dinuclear or mononuclear complexes and not oligomers owing to the low coordination ability of the cationic ligand. Sulfide sulfur generally has a stronger coordination ability to Ru ions than the cyano group. Therefore, ILs with dialkylsulfide substituents may produce bridged structures with higher thermal stability upon photoirradiation. However, their products might be susceptible to C–S bond cleavage.

*2.6. Ionic Conductivity of **1-FTA***

The ionic conductivity of **1-FTA** decreased after UV photoirradiation owing to the photochemical reaction. The ionic conductivity of **1-FTA** was 8.8×10^{-4} S cm^{-1} at 25 °C, which was lower than those of typical imidazolium ILs (*e.g.*, 4.1×10^{-3} S cm^{-1} for [Bmim]Tf_2N [15]) but higher than those of Ru-containing organometallic ILs with other anions (*e.g.*, 4.0×10^{-4} S cm^{-1} for **2-FSA** [6b]) owing to its low viscosity. Upon UV irradiation for 70 min, the ionic conductivity of the IL decreased to 8.7×10^{-5} S cm^{-1} (Fig. 8a). This is consistent with the formation of product A, which is accompanied by a decrease in the number of carrier ions and an increase in viscosity. As seen in Fig. 8a, the photoreaction was slower than that of **2-FSA**. The magnitude of the conductivity change of **1-FTA** was similar to that of **2-FSA** (4.0×10^{-4} S cm^{-1} to 3.7×10^{-5} S cm^{-1} [6b]) despite the lower reaction rate of **1-FTA** (suggested 43% yield of product A) than that of **2-FSA** (93%). This is probably because the anion in **1-FTA** is bound to the photoproduct, whereas the anion in **2-FSA** is free after the photoreaction.

The intermediate formed after heating the photoproduct at 120 °C for 1 h exhibited an ionic conductivity of 1.7 × 10^{-4} S cm^{-1}. This value was between those before and after photoirradiation, which is coherent considering the dissociation of product A. Further heating of the photoproduct at 200 °C for 3 min increased its ionic conductivity to 2.1 × 10^{-4} S cm^{-1}. This value was slightly lower than the initial value, which might be owing to slight decomposition.

The temperature dependence of the ionic conductivity of **1-FTA** before and after photoirradiation was measured (Fig. 8b). The data before photoirradiation were fitted using the Vogel–Fulcher–Tamman (VFT) equation [16]:

$$\sigma(T) = \frac{\mathrm{A}}{\sqrt{T}} \exp\left(\frac{-E_a}{k_B(T-T_0)}\right),$$

where A is proportional to the number of carrier ions in the matrix, and E_a and T_0 are the activation energy for ion transport and the ideal glass transition temperature, respectively. The obtained values of these parameters were E_a = 162(19) meV, A = 623(319) S $K^{1/2}$ cm^{-1}, and T_0 = 122(12) K, where the values in parentheses are the standard deviations. The data after photoirradiation were fitted using the Arrhenius equation $\sigma(T) = \sigma_\infty \exp(-E_a/k_B T)$ [17] (E_a = 730(12) meV and σ_∞= 2.2(0.9) × 10^8 S cm^{-1}) and indicated a linear relationship. However, the plot deviated from the straight line above 60 °C owing to the thermal reaction. The larger activation energy after photoirradiation was consistent with the higher viscosity and larger molecules of product A.

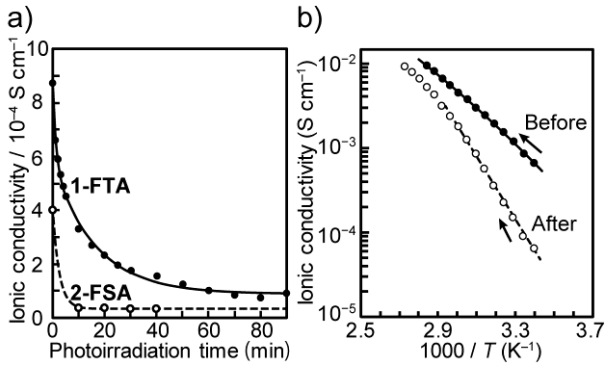

Fig. 8. (a) Change in ionic conductivities of **1-FTA** (solid line) and **2-FSA** (dashed line [6b]) as a function of photoirradiation time. (b) Temperature dependence of ionic conductivity of **1-FTA** before (●) and after (○) photoirradiation. The solid and dashed lines in (b) indicate the fitting with the VFT and Arrhenius equations, respectively.

3. Conclusion

Ru-containing organometallic ILs with sulfur-containing substituents were synthesized. The FSA and PF_6 salts exhibited relatively high melting points, and the high melting point of the former was attributed to its dense crystal packing. The FSA salt underwent an order–disorder phase transition of the anions and cations at low temperatures. The FTA salt was in the liquid state, which indicated that the unsymmetric anion is effective for obtaining Ru-containing organometallic ILs with low melting points.

The FTA salt underwent structural transformation upon UV photoirradiation, which resulted in a more viscous liquid. The product transformed back to the original IL via an intermediate state upon heating, and the corresponding changes in ionic conductivity were evaluated. The photoreactivity and conversion of **1-FTA** were lower than those of structurally similar ILs with cyano substituents. Furthermore, the photoproducts of **1-FTA** were likely dinuclear or mononuclear complexes and not oligomers. This study demonstrated that the photochemical reactivity of the Ru-containing organometallic ILs strongly depend on the donor atom. Other donor atoms to achieve rapid photoreaction rates and higher thermal stabilities of the photoproducts are being investigated in our laboratory. These studies are significant for the development of stimuli-responsive ILs for their application in electronic devices.

4. Experimental

4.1. General

$[CpRu(CH_3CN)_3]PF_6$ was synthesized according to a previously reported method [7]. Butylthiobenzene was synthesized by the reaction of thiophenol and 1-bromobutane in methanol (yield 89%) [18]. Other reagents were purchased from TCI Co. (Tokyo, Japan). ^1H and ^{19}F NMR spectroscopy were carried using a Bruker Avance 400 spectrometer and FT-IR spectroscopy using a Thermo Nicolet iS5 spectrometer equipped with an attenuated total reflectance unit (ATR, diamond). UV-vis absorption spectroscopy was conducted using a JASCO V-570 UV/VIS/NIR spectrophotometer. DSC measurements were performed using a TA Instruments Q100 differential scanning calorimeter at scan rates of 10 and 5 °C min^{-1} using aluminum hermetic pans as sample containers. TG-DTA measurements were performed using a Rigaku TG8120 thermal analyzer at a scan rate of 10 K min^{-1} under a nitrogen atmosphere. GPC was performed using a Recycling Preparative HPLC system (LC908, Japan Analytical Industry) equipped with JAIGEL-2HR (eluent: chloroform). ESI-MS spectroscopy was carried out using a Thermo Fisher Scientific LTQ-Orbitrap Discovery instrument. The ionic conductivities were measured using a Solartron 1260 impedance analyzer. The sample was sandwiched between a gold interdigitated electrode (gap dimension: 200 μm) and a quartz plate and sealed with epoxy resin. A Japan High Tech 10013 L heating/cooling stage was used for temperature control. A Hamamatsu LC-L1V3 Lightning Cure UV-LED (LED lamp, wavelength: 365 nm, intensity: 650 mW cm^{-2}) was used for UV photoirradiation. The photoirradiation was conducted at 10 °C on samples sandwiched between two quartz plates or sealed in the electrode cells for conductivity measurements. The ratio of the photodissociated cations was determined from the ^1H NMR spectra (CD_3CN).

*4.2. Synthesis of $[CpRu(PhSBu)]PF_6$ (**1-PF$_6$**)*

$[CpRu(NCCH_3)_3]PF_6$ (303 mg, 0.70 mmol) was dissolved in acetonitrile (10 mL) in a nitrogen atmosphere. Then, butylthiobenzene (162 mg, 0.97 mmol) was added to the solution

and stirred at 90 °C for 24 h. The resultant solution was evaporated under reduced pressure, and the residue was dissolved in a small amount of acetonitrile. The solution was charged to an alumina column, and unreacted ligand was eluted with hexane. Then the desired compound was eluted with acetonitrile. The solvent was evaporated and the residue dried under vacuum. The residue was recrystallized from acetone–diethyl ether by slow cooling to −60 °C and then collected by filtration. A few black and solid impurities were observed using a microscope and were subsequently removed. The desired product was obtained as a white needle-shaped crystal (131 mg, 39%). ^{1}H NMR (400 MHz, $CDCl_3$): δ = 0.97 (t, 3H, *CH*$_3$, *J* = 7.32 Hz), 1.49 (sext, 2H, SCH_2CH_2*CH*$_2$, *J* = 7.68 Hz), 1.69 (quint, 2H, SCH_2*CH*$_2$$CH_2$, *J* = 7.64 Hz), 3.00 (t, 2H, S*CH*$_2$$CH_2CH_2$, *J* = 7.36 Hz), 5.39 (s, 5H, Cp-*H*$_5$), 6.11 (t, 1H, Ar-*H*$_1$, *J* = 5.68 Hz), 6.21 (t, 2H, Ar-*H*$_2$, *J* = 6.32 Hz), 6.27 (d, 2H, Ar-*H*$_2$, *J* = 5.88 Hz). FT-IR (ATR, cm^{-1}): 567, 728 (S–F), 824, 1088 (C–C), 1179 (S=O), 1363 (S=O), 1418 (Cp, C–H), 1503 (C=C), 2871, 2932, 2954, 3092 (C–H). Anal. Calcd. for $C_{15}H_{19}F_6PRuS$: C, 37.7, H, 4.01, N, 0.00. Found: C, 37.8, H, 4.17, N, 0.03.

*4.3. Synthesis of [CpRu(PhSBu)]FSA (**1-FSA**)*

An aqueous solution of K[FSA] (178 mg, 0.812 mmol) was added to a solution of [CpRu(PhSBu)]PF_6 (128 mg, 0.268 mmol) in acetone and stirred for 20 min. Then, acetone was evaporated under reduced pressure, followed by the addition of water and dichloromethane to the residue. The residue was extracted five times using dichloromethane, and the obtained combined organic layer was dried using anhydrous magnesium sulfate. The anion exchange procedure was repeated and the complete exchange of PF_6 was confirmed by the absence of the PF_6 peak (δ = −73.83, −71.92) in the ^{19}F NMR spectrum (solvent: CD_3CN). Subsequently, the residue was recrystallized from acetone–diethyl ether by slow cooling to −60 °C. The desired product was obtained as white needle-shaped crystals (88 mg, 64%).^{1}H NMR (400 MHz,

CD_3CN): δ = 0.98 (t, 3H, *CH₃*, *J* = 7.36 Hz), 1.49 (sext, 2H, $SCH_2CH_2CH_2$, *J* = 7.68 Hz), 1.70 (quint, 2H, $SCH_2CH_2CH_2$, *J* = 7.52 Hz), 3.02 (t, 2H, $SCH_2CH_2CH_2$, *J* = 7.48 Hz), 5.34 (s, 5H, Cp-*H₅*), 6.01 (t, 1H, Ar-*H₁*, *J* = 5.72 Hz), 6.11 (t, 2H, Ar-*H₂*, *J* = 6.4 Hz), 6.28 (d, 2H, Ar-*H₂*, *J* = 5.92 Hz). FT–IR (ATR, cm^{-1}): 569, 601, 721 (S–F), 759, 805, 848, 1074 (C–C), 1146 (S=O), 1181, 1337, 1370 (S=O), 1418 (Cp, C–H), 1504 (C=C), 2874, 2933, 2962, 3112 (C–H). Anal. Calcd. for $C_{15}H_{19}F_2NO_4RuS_3$: C, 35.15, H, 3.74, N, 2.73. Found: C, 35.49, H, 3.47, N, 2.87.

*4.4. Synthesis of [CpRu(PhSBu)]FTA (**1-FTA**)*

Anion exchange was conducted as described for **1-FSA** using Li[FTA] (80 mg, 0.337 mmol) and $[CpRu(PhSBu)]PF_6$ (70.3 mg, 0.147 mmol). The procedure was repeated three times, and the crude product was purified by passing it through a short alumina column (eluent: acetonitrile). After the solvent was evaporated, the residue was heated under vacuum at 60 °C for 15 h. The desired product was obtained as a pale orange liquid (78 mg, 94%). ^{1}H NMR (400 MHz, CD_3CN): δ = 0.98 (t, 3H, *CH₃*, *J* = 7.36 Hz), 1.50 (sext, 2H, $SCH_2CH_2CH_2$, *J* = 7.6 Hz), 1.70 (quint, 2H, $SCH_2CH_2CH_2$, *J* = 7.56 Hz), 3.02 (t, 2H, $SCH_2CH_2CH_2$, *J* = 7.48 Hz), 5.34 (s, 5H, Cp-*H₅*), 6.02 (t, 1H, Ar-*H₁*, *J* = 5.72 Hz), 6.12 (t, 2H, Ar-*H₂*, *J* = 6.32 Hz), 6.29 (d, 2H, Ar-*H₂*, *J* = 5.88 Hz). ^{19}F NMR (400 MHz, CD_3CN): δ = –79.3, 55.6. FT–IR (ATR, cm^{-1}): 721 (C–S), 759, 805, 848, 1074 (C–C), 1146, 1181, 1337, 1370 (S=O), 1418 (Cp, C–H), 1504 (C=C), 2874, 2933, 2962, 3112 (C–H). Anal. Calcd. for $C_{16}H_{19}F_4NO_4RuS_3$: C, 34.16; H, 3.40; N, 2.49. Found: C, 34.53; H, 3.40; N, 2.10.

4.7. X-ray crystallography

Crystals of **1-PF₆** and **1-FSA** suitable for structural analysis were obtained by recrystallization from acetone–diethyl ether by slow cooling to −60 °C. Single crystal X-ray diffraction data were collected using Bruker APEX II Ultra (X-ray source: MoKα). Calculations

were performed using SHELXL [19]; the crystallographic parameters are listed in Table S1 (Supporting Information). Packing indices were calculated using the Platon software [20]. CCDC 2052308 (**1-PF_6**), 2059258 (**1-FSA**, −183 °C), and 2063565 (**1-FSA**, 0 °C) contain the crystallographic data pertaining to this work. These data can be obtained free of charge via www.ccdc.cam.ac.uk/data_request/cif.

CRediT authorship contribution statement

Ryo Sumitani: Investigation, Visualization, Writing - review & editing. **Tomoyuki Mochida:** Conceptualization, Writing - original draft, Writing - review & editing.

Declaration of competing interest

The authors declare that they have no known competing financial interests or personal relationships that could have appeared to influence the work reported in this paper.

Acknowledgments

We thank Mr. Yuya Okada (Kobe Univ.) for the preparation of the salts. This work was financially supported by KAKENHI (grant number 20H02756) from the Japan Society for the Promotion of Science (JSPS).

Appendix A. Supplementary data

Supplementary data to this article can be found online at https://doi.org/

References

[1] M. Kar, K. Matuszek, D. R. MacFarlane, Kirk-Othmer Encyclopedia of Chemical Technology, John Wiley & Sons, Inc (2019), doi:10.1002/0471238961.ionisedd.a01.pub2.

[2] a) N. R. Brooks, S. Schaltin, K. Van Hecke, L. Van Meervelt, K. Binnemans, J. Fransaer,

Chem. Eur. J. 17 (2011) 5054–5059, https://doi.org/10.1002/chem.201003209;

b) M. Iida, C. Baba, M. Inoue, H. Yoshida, E. Taguchi, H. Furusho, Chem. Eur. J. 14 (2008) 5047–5056, https://doi.org/10.1002/chem.200701764;

c) P. Zhang, Y. Gong, Y. Lv, Y. Guo, Y. Wang, C. Wang, H. Li, Chem. Commun. 48 (2012) 2334–2336, https://doi.org/10.1039/C2CC16906A;

d) S. A. Pierson, O. Nacham, K. D. Clark, H. Nan, Y. Mudryk, J. L. Anderson, New J. Chem. 41 (2017) 5498–5505, https://doi.org/10.1039/C7NJ00206H;

e) Y. Yoshida, G. Saito, in Ionic Liquids: Theory, Properties, New Approaches, ed. A. Kokorin, IntechOpen, 2011, 723–738, https://doi.org/10.5772/14846.

[3] a) T. Tominaga, T. Mochida, Chem. Eur. J. 24 (2018) 6239–6247, https://doi.org/10.1002/chem.201800333;

b) A. Komurasaki, Y. Funasako, T. Mochida, Dalton. Trans. 44 (2015) 7595–7605, https://doi.org/10.1039/C5DT00723B;

c) T. Inagaki, T. Mochida, M. Takahashi, C. Kanadani, T. Saito, D. Kuwahara, Chem. Eur. J. 18 (2012), 6795–6804, https://doi.org/10.1002/chem.201200151;

d) Y. Funasako, T. Mochida, T. Inagaki, T. Sakurai, H. Ohta, K. Furukawa, T. Nakamura, Chem. Commun. 47 (2011) 4475–4477, https://doi.org/10.1039/C0CC05820C.

[4] a) X. Lan, T. Mochida, Y. Funasako, K. Takahashi, T. Sakurai, H. Ohta, Chem. Eur. J. 23 (2017) 823–831, https://doi.org/10.1002/chem.201604420;

b) Y. Funasako, T. Mochida, K. Takahashi, T. Sakurai, H. Ohta, Chem. Eur. J. 18 (2012) 11929–11936, https://doi.org/10.1002/chem.201201778;

c) M. Okuhata, Y. Funasako, K. Takahashi, T. Mochida, Chem. Commun. 49 (2013) 7662–7664, https://doi.org/10.1039/C3CC44199G

[5] a) J. Cui, Y. Li, D. Chen, T.-G. Zhan, K.-D. Zhang, Adv. Funct. Mater. 30 (2020) 2005522, https://doi.org/10.1002/adfm.202005522;

b) Y. Yoshida, H. Kitagawa, ACS Appl. Electron. Mater. 3 (2021) 2468–2482, https://doi.org/10.1021/acsaelm.1c00334.

[6] a) Y. Funasako, S. Mori, T. Mochida, Chem. Commun. 52 (2016) 6277–6279, https://doi.org/10.1039/C6CC02807A;

b) R. Sumitani, H. Yoshikawa, T. Mochida, Chem. Commun. 56 (2020) 6189–2040, https://doi.org/10.1039/D0CC02786C;

c) R. Sumitani, Y. Funasako, T. Mochida, J. Mol. Liq. 318 (2020) 114071, https://doi.org/10.1016/j.molliq.2020.114071;

d) T. Ueda, T. Tominaga, T. Mochida, K. Takahashi, S. Kimura, Chem. Eur. J., 24 (2018) 9490–9493, https://doi.org/10.1002/chem.201801365.

[7] a) T. P. Gill, K. R. Mann, Organometallics 1 (1982) 485–488, https://doi.org/10.1021/om00063a014;

b) B. M. Trost, C.M. Older, Organometallics 21 (2002) 2544–2546, https://doi.org/10.1021/om020143p.

[8] a) R. Sumitani, T. Mochida, Macromolecules 53 (2020) 6968–6974, https://doi.org/10.1021/acs.macromol.0c01141:

b) R. Sumitani, T. Mochida, Soft Matter. 16 (2020) 9946–9954, https://doi.org/10.1039/D0SM01567A;

c) R. Fan, R. Sumitani, T. Mochida, ACS Omega 5 (2020) 2034–2040, https://doi.org/10.1021/acsomega.9b04272

[9] H. Matsumoto, N. Terasawa, T. Umecky, S. Tsuzuki, H. Sakaebe, K. Asaka, K. Tatsumi, Chem. Lett. 37 (2008) 1020–1021, https://doi.org/10.1246/cl.2008.1020.

[10] a) O. Yamamuro Y. Minamimoto Y. Inamura S. Hayashi H. Hamaguchi, Chem. Phys. Lett. 423 (2006) 371–375, https://doi.org/10.1016/j.cplett.2006.03.074;

b) D. Turnbull, M. H. Cohen, J. D. Mackenzie, Modern Aspect of the Vitreous State I (1960)

Butterworth London pp. 38.

[11] T. Tominaga, T. Ueda, T. Mochida, Phys. Chem. Chem. Phys. 19 (2017) 4352–4359, https://doi.org/10.1039/C6CP08308K.

[12] a) T. Higashi, T. Ueda, T. Mochida, Phys. Chem. Chem. Phys. 18 (2016) 10041–10048, https://doi.org/10.1039/C6CP00643D;

b) T. Ueda, T. Mochida, Organometallics 34 (2015) 1279–1286, https://doi.org/10.1021/acs.organomet.5b00021.

[13] a) K. Matsumoto, T. Oka, T. Nohira, R. Hagiwara, Inorg. Chem. 52 (2013) 568–576, https://doi.org/10.1021/ic3010486;

b) T. Mochida, Y. Funasako, T. Inagaki, M. Jiao Li, K. Asahara, D. Kuwahara, Chem. Eur. J. 19 (2013) 6257–6264, https://doi.org/10.1002/chem.201300186.

[14] D. B. Williams, M. E. Stoll, B. L. Scott, D. A. Costa, W. J. Oldham Jr., Chem. Commun. (2005) 1438–1440, https://doi.org/10.1039/B416830E.

[15] J. A. Widegren, E. M. Saurer, K. N. Marsh, J. W. Magee, J. Chem. Thermodyn. 37 (2005) 569–575, https://doi.org/10.1016/j.jct.2005.04.009.

[16] a) H. Vogel, Phys. Z. 22 (1921) 645–646;

b) G.S. Fulcher, J. Am. Ceram. Soc. 8 (1925) 339–355, https://doi.org/10.1111/j.1151-2916.1925.tb16731.x;

c) G. Tammann, W. Hesse, Allg. Chemie 156 (1926) 245–257, https://doi.org/10.1002/zaac.19261560121.

[17] a) M. Petrowsky, R. Frech, J. Phys. Chem. B 114 (2010) 8600–8605, https://doi.org/10.1021/jp1020142;

b) H. Every, A. G. Bishop, M. Forsyth, D. R. MacFarlane, Electrochim. Acta 45 (2000) 1279–1284, https://doi.org/10.1016/S0013-4686(99)00332-1.

[18] H. Leicht, I. G. Schnetmann, S. Mecking, J. Am. Chem. Soc. 139 (2017) 6823–6826,

https://doi.org/10.1021/jacs.7b03087.

[19] G. M. Sheldrick, Acta Cryst. A 64 (2008) 112–122, https://doi.org/10.1107/S0108767307043930.

[20] A. L. Spek, Acta Cryst. D 65 (2009) 148–155, https://doi.org/10.1107/S090744490804362X.

Supporting Information

Thermal Properties, Crystal Structures, and Photoreactivity of Ru-Containing Ionic Liquids with Sulfur-Containing Substituents

Ryo Sumitani[a] and Tomoyuki Mochida[a,b]*

[a]*Department of Chemistry, Graduate School of Science, Kobe University, 1-1 Rokkodai, Nada, Kobe, Hyogo 657-8501, Japan*

[b]*Research Center for Membrane and Film Technology, Kobe University, 1-1 Rokkodai, Nada, Kobe, Hyogo 657-8501, Japan*

Contents

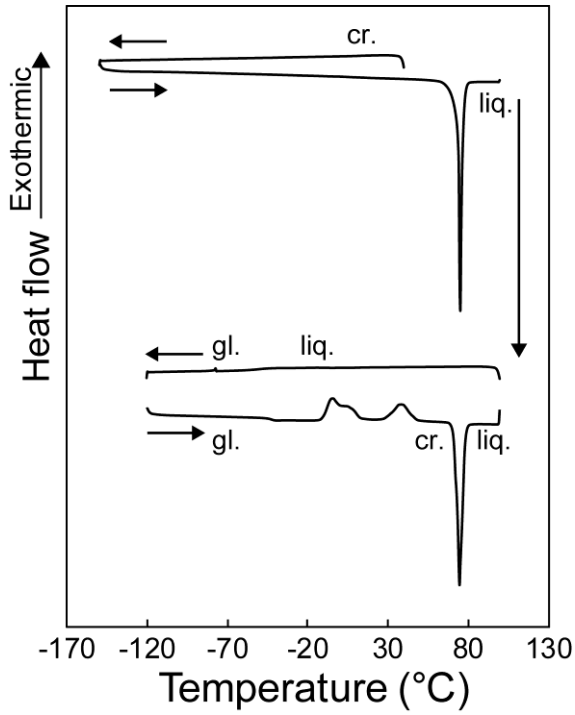

Fig. S1. DSC curves of **1-PF$_6$**, where cr., liq., and gl. are the crystal, liquid, and glassy states, respectively.

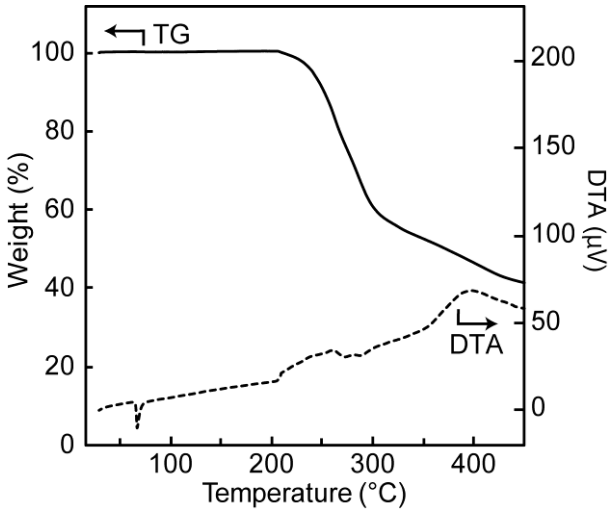

Fig. S2. TG–DTA traces of **1-FSA** measured under a nitrogen atmosphere at 10 K min^{-1}. The TG and DTA curves are represented by solid and dashed lines, respectively.

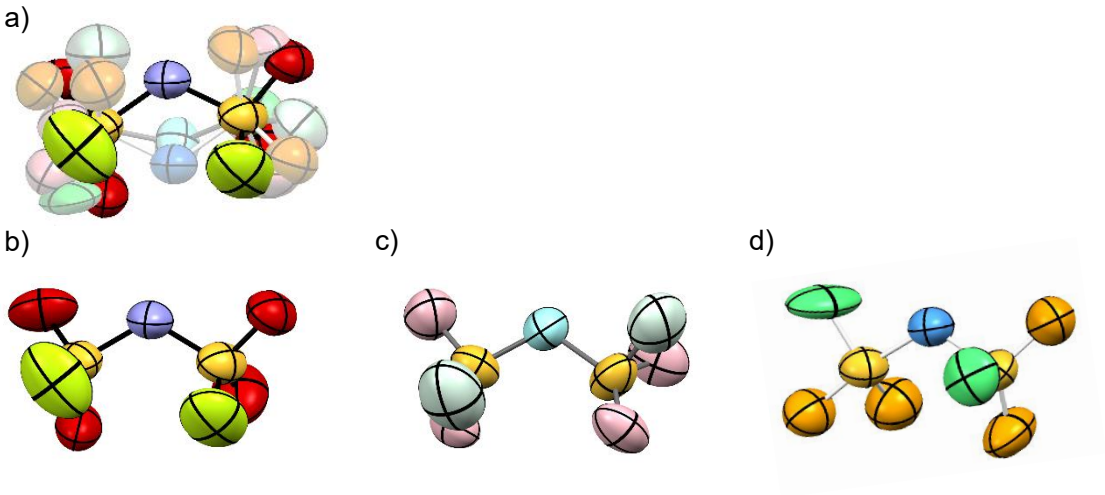

Fig. S3. Structure of the anion in the **1-FSA** crystal at 0 °C. (a) Disorder structure and (b–d) three components of the disorder, whose occupancies are 0.53, 0.27, and 0.20, respectively.

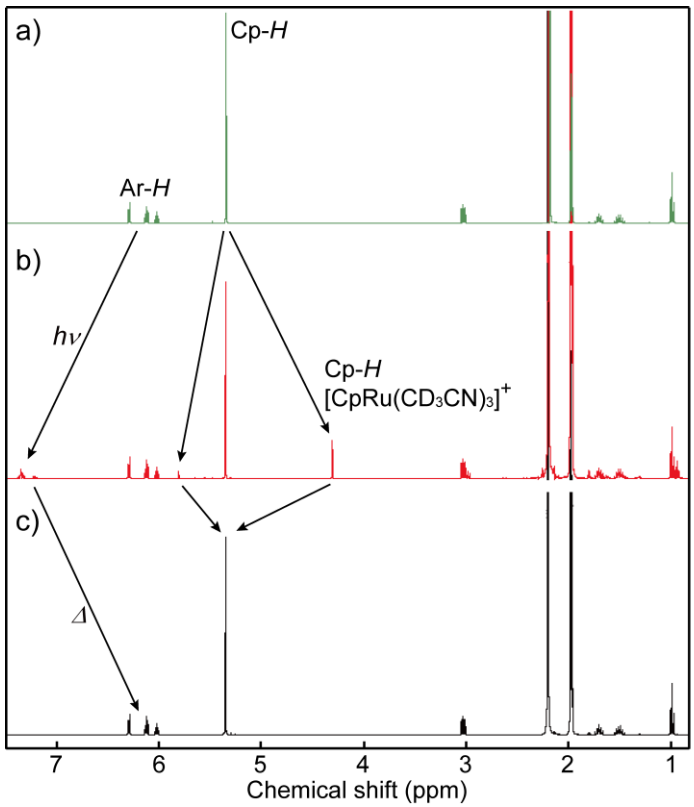

Fig. S4. ^{1}H NMR spectra (in CD_3CN) of **1-FTA** (a) before and (b) after photoirradiation for 90 min and (c) after heating the photoproduct at 200 °C for 1 min. In CD_3CN, weakly coordinated ligands dissociate from the half-sandwich complexes to produce solvent-coordinated complexes such as $[CpRu(CD_3CN)_3]^+$ and $[CpRu(PhSBu)(CD_3CN)_2]^+$.

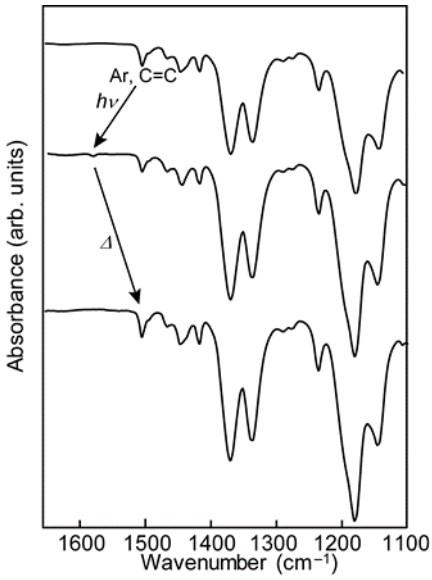

Fig. S5. Changes in FT-IR spectra observed upon photoirradiation of **1-FTA** for 90 min and after successive heating of the photoproduct at 200 °C for 1 min.

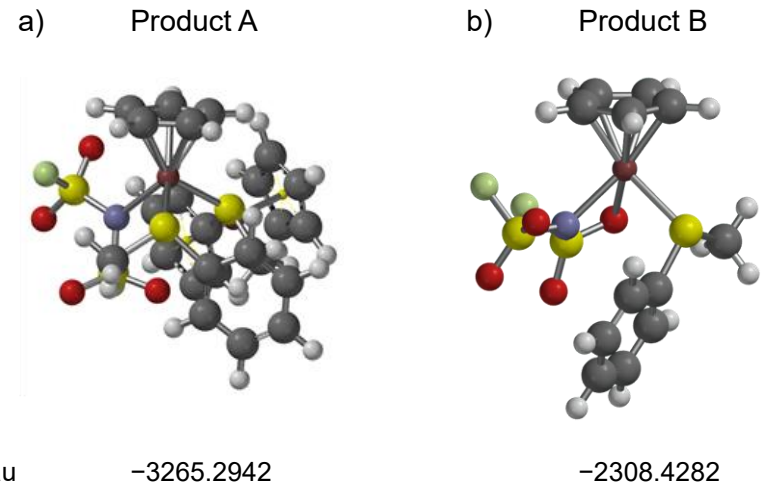

Fig. S6. Optimized geometries of products A and B obtained using DFT calculations (B97-D/LanL2DZ). The butyl group of the cation was replaced with a methyl group for the calculations.

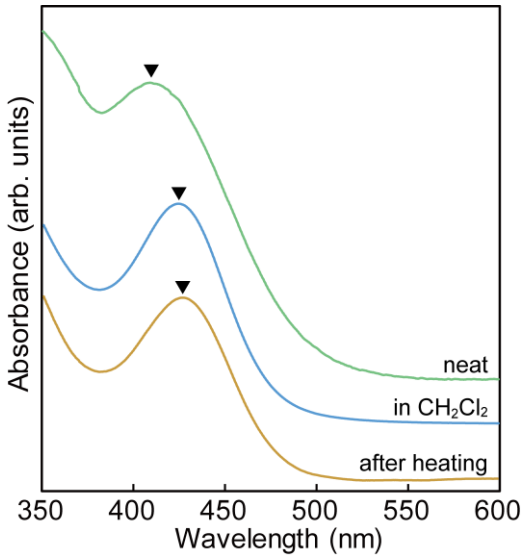

Fig. S7. UV-vis spectra of the photoproduct of **1-FTA** in the neat state (top), in CH_2Cl_2 solution (middle), and in the neat state after heating at 120 °C for 5 min (bottom).

Table S1. Crystallographic parameters

	1-PF$_6$ (−183 °C)	**1-FSA** (−183 °C)	**1-FSA** (0 °C)
Empirical formula	$C_{15}H_{19}F_6PRuS$	$C_{15}H_{19}F_2NO_4RuS_3$	$C_{15}H_{19}F_2NO_4RuS_3$
Formula weight	477.4	512.56	512.56
Crystal system	triclinic	triclinic	triclinic
Space group	$P\bar{1}$	$P\bar{1}$	$P\bar{1}$
a [Å]	7.528(3)	7.7168(19)	7.8377(9)
b [Å]	9.202(3)	9.370(2)	9.5249(11)
c [Å]	12.616(5)	13.320(3)	13.5742(16)
α [°]	84.052(4)	90.778(3)	91.711(2)
β [°]	73.771(4)	97.877(3)	98.3740(10)
γ [°]	89.723(4)	102.049(3)	102.0820(10)
V [Å^3]	834.3(5)	932.1(4)	978.4(2)
Z	2	2	2
ρ_{calcd} [g cm^{-3}]	1.9	1.826	1.740
μ [mm^{-1}]	1.217	1.217	1.160
Temperature [K]	90	90	273
F(000)	476	516	516
Reflns collected	4144	5015	9961
R (int)	0.0184	0.0106	0.0128
Goodness of fit	1.067	1.053	1.061
R_1[a], R_w[b] ($I > 2\sigma$)	0.0184	0.024	0.0356
R_1[a], R_w[b] (all data)	0.0189	0.0252	0.0988

[a] $R_1 = \Sigma||F_o| - |F_c|| / \Sigma|F_o|$. [b] $R_w = [\Sigma w (F_o^2 - F_c^2)^2 / \Sigma w (F_o^2)^2]^{1/2}$